ACS OMEGA

http://pubs.acs.org/journal/acsodf

Article

Custom Synthesis of ZnO Nanowires for Efficient Ambient Air-Processed Solar Cells

Ali Nourdine,* Marwen Abdelli, Nicolas Charvin, and Lionel Flandin

Cite This: *ACS Omega* 2021, 6, 32365−32378

Read Online

ACCESS | Metrics & More | Article Recommendations

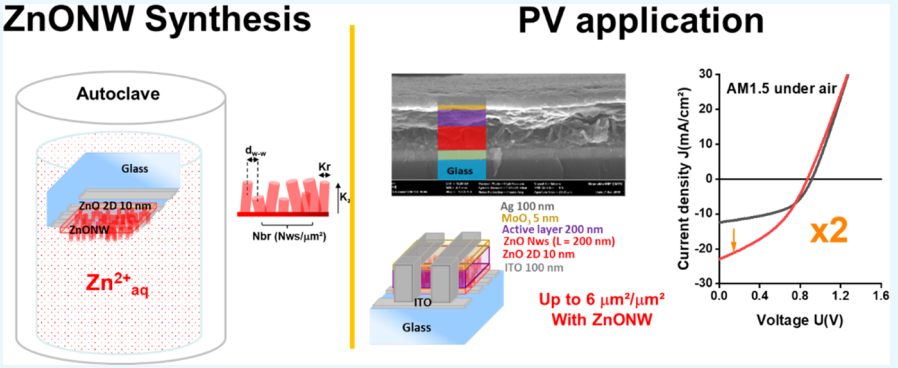

ABSTRACT: Nanostructuration of solar cells is an interesting approach to improve the photovoltaic conversion efficiency (PCE). This work aims at developing architectured 3D hybrid photovoltaic solar cells using ZnO nanowires (ZnONWs) as the electron transport layer (ETL) and nanocollectors of electrons within the active layer (AL). ZnONWs have been synthesized using a hydrothermal process with a meticulous control of the morphology. The AL of solar cells is elaborated using ZnONWs interpenetrated with a bulk heterojunction composed of donor (π-conjugate low band gap polymer: PBDD4T-2F)/acceptor (fullerene derivate: $PC_{71}BM$) materials. An ideal interpenetrating ZnONW-D/A system with predefined specific morphological characteristics (length, diameter, and inter-ZnONW distances) was designed and successfully realized. The 3D architectures based on dense ZnONW arrays covered with conformal coatings of AL result in an increased amount of the ETL/AL interface, enhanced light absorption, and improved charge collection efficiency. For AL/ZnONW assembly, spin-coating at 100 °C was found to be the best. Other parameters were also optimized such as the D/A ratio and the pre/post-treatments achieving the optimal device with a D/A ratio of 1.25/1 and methanol treated on ZnONWs before and after the deposition of AL. A PCE of 7.7% (1.4 times better than that of the 2D cells) is achieved. The improvement of the performances with the 3D architecture results from both of: (i) the enhancement of the ZnO/AL surface interface (1 $\mu m^2/\mu m^2$ for the 2D structure to 6.6 $\mu m^2/\mu m^2$ for the 3D architecture), (ii) the presence of ZnONWs inside the AL, which behave as numerous nanocollectors (~60 ZnONW/μm^2) of electrons in the depth of the AL. This result validates the efficiency of the concept of nanotexturing of substrates, the method of solar cell assembly based on the nano-textured surface, the chosen morphological characteristics of the nanotexture, and the selected photoactive organic materials.

1. INTRODUCTION

Organic and hybrid photovoltaic (OPV and HPV) technologies have emerged as alternatives to the first (silicon) and second generation (semiconducting inorganic materials) solar cells, leading to the fabrication of less-expensive devices. Perovskites (organometallic), all OPV, and organic/inorganic HPV are developed specifically for nomad applications. Emerging HPV materials are of special interest because they combine the low cost and large-scale production advantages of polymers or other organic materials with charge carrier mobility and inorganic materials with chemical stability. The OPV cells or organic parts of hybrid cells are always made with the combination of two distinct components, namely the electron-accepting (acceptor A) and the hole-accepting (donor D) materials. There have already been reports on large varieties of these materials, such as π-conjugated wide[1,2] and low-band[3−5] gap polymers, fullerene C_{60} or C_{70} derivatives,[6] and nonfullerene acceptors[7] such as ITIC.[3]

The development of PV devices essentially relies on nanomaterials or nanostructures with specific properties and

Received: March 27, 2021
Accepted: May 27, 2021
Published: June 25, 2021

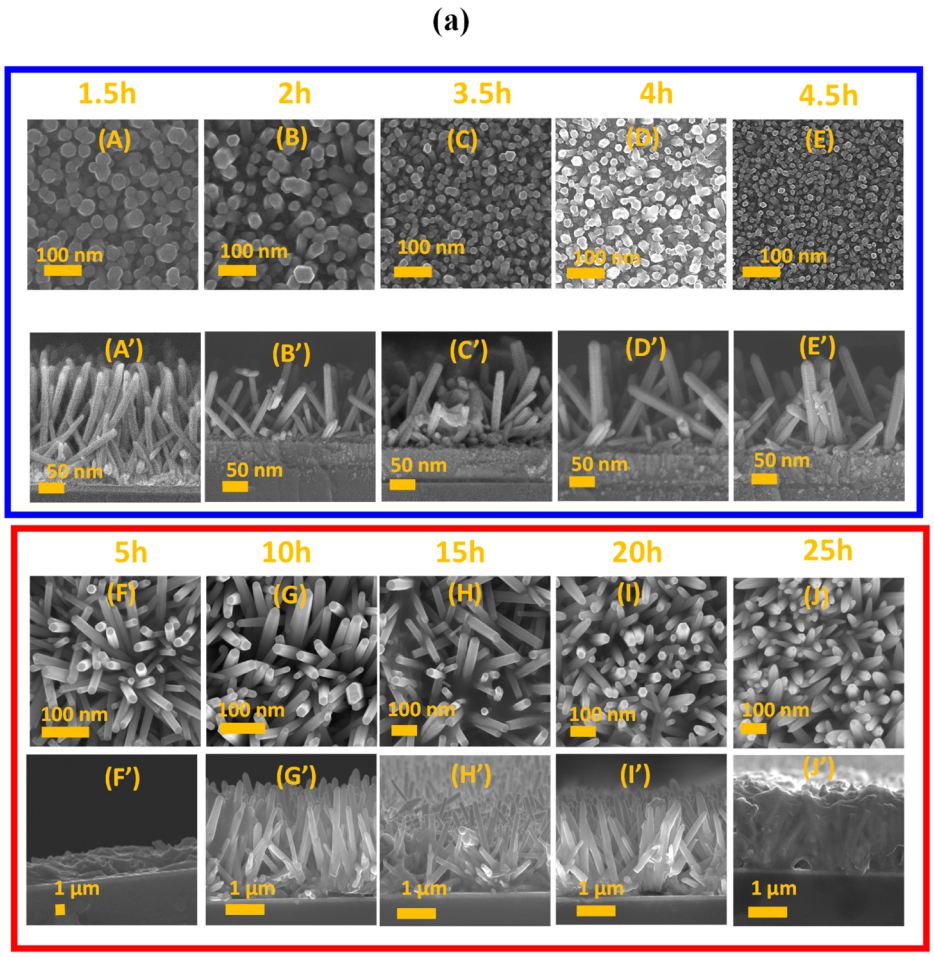

Figure 1. (a) SEM images of ZnONW samples at various growth times, (A–J) top surface view and (A′–J′) cross-sectional view. (b) Morphological properties of synthesized ZnONWs as a function of growth time: average length (brown □), average diameter (orange ○), aspect ratio (green ☆), and areal number density (gray ◊).

https://doi.org/10.1021/acsomega.1c01654
ACS Omega 2021, 6, 32365−32378

dedicated morphologies for all kinds of solar cells: organic,[8−11] inorganic,[12−14] hybrid,[15] dye-sensitized,[16] and perovskite.[17] Controlling the structure at the nanoscale allows mastering the physical phenomena of carrier charge transport and electronic or optical confinement.[18] Adjusting the morphology and the domain sizes close to the critical distances in the D/A heterojunction improves the local PV efficiency and consequently the global performances of devices. Following the same approach, ZnONWs have been developed in this work as local nanocollectors of electrons within the active layer (AL). ZnO was chosen as the carrier material of the nanostructure. It is widely used as a functional material in several optoelectronic applications such as light-emitting diodes (LEDs),[19] dye PV cells,[20−23] sensors,[24,25] thermoelectric devices,[26] transistors,[27] photoelectrodes,[28,29] and photo-assisted batteries[30] because it presents a unique combination of functional properties, structural properties, chemical stability, and tunable micro/nanostructure.[22,31] In terms of functional properties, semiconducting ZnO has an optical gap of 3.37 eV at 300 K,[32] a resistivity of 10^{-4} Ω Cm, and an electronic mobility between 10 and 60 $cm^2\ s^{-1}\ V^{-1}$ depending on the microstructure.[33] At the atomic scale, ZnO can crystallize in three different forms: cubic (rocksalt), face-centered cubic (blende), and compact hexagonal (wurtzite). The latter is the most favorable and stable during the synthesis.[32] At the nano/microscale, ZnO allows preparing a large variety of nanostructures and microstructures such as nanorods, nanotubes, nanorings, nanospirals, nanosprings, nanohelices, nanobows, branched nanowires, and nanowalls.[14,16,34,35] The applicability of ZnO in PV cells has already been established. The literature essentially concerns ZnONWs with a micrometric length and a nanometric diameter.[35−38] A few studies also reported the production of nanowire structures by an electrochemical route[39] or chemical bath deposition.[40] The current work suggests a direct path to the custom synthesis of ZnONWs with tunable morphological characteristics and nanometric dimensions (length and diameter). The hydrothermal synthesis was chosen, and optimized and simplified for the reproducible fabrication of tailored nano-ordered ZnO structures. They could further be used to prepare nano-architectured solar cells. The assembly of solar cells based on rough ZnONWs requires specific processing conditions, in addition to the usual deposition techniques at the laboratory scale, including spin-coating and doctor blade.[41] Other several processing conditions were also reported in the literature, such as immersion at atmospheric pressure,[42] drop-casting,[43] vacuum-assisted coating.[44]

ZnO 3D-like nanostructures are currently being used in solar PV technologies such as ETL and photoelectrodes[45] to enhance the PV performances of dye-sensitized, organic, or perovskite solar cells.[22,46,47] Despite the morphological properties of ZnO (nanostructures, their dimensions, and aspect ratio) and the preparation method, the functionality and performances of a 3D-ZnO-based device depend also on the intrinsic properties (i.e., charge mobility, absorption, energy levels, so forth of photoactive materials used in the AL and in the ETL/AL interface (i.e., absorber) and the processing conditions. For organic devices, it was demonstrated in the literature that, when optimal photoactive materials are meticulously selected, high performances are achievable with ZnONW/D/A or ZnONW/absorber/D systems compared to simple ZnONW/D systems.[22]

This work focuses on the (i) use of efficient photoactive materials with functional properties compatible with ZnO and (ii) the exploitation of a nano-structured 3D architecture in PV solar cells. The geometrical organization relies on ZnONWs grown by a hydrothermal route on the solar cell substrate (glass/ITO). The organic part is a D/A heterojunction composed of low band gap polymer PBDD4T-2F and $PC_{71}BM$ as a donor and an acceptor, respectively.[48] The design consisting of an optimal interpenetration between the D/A heterojunction and the ZnONW network incorporated in the AL theoretically corresponds to an ideal architecture.[49] Even the dimensions of the heterogeneities were chosen to match the critical distances for exciton diffusion and free charge carrier transport.[50,51]

2. RESULTS AND DISCUSSION

2.1. Synthesis of ZnONWs. The hydrothermal synthesis of ZnO consists in making ZnO nanoparticles grow by controlled precipitation in an alkaline medium of predissolved zinc salt ($Zn(NO_3)_2$) in the presence of a nonionic amine hexamethylenetetramine (HMTA), which facilitates the anisotropic growth in the 001 direction.[52] For the optimization of the synthetic route of ZnONWs, the temperature, the precursors' concentrations, pH, the thickness, and the producing method of the seed layer were fixed. These parameters were chosen from the optimum values described in the literature.[53−56] In order to optimize the morphology of the ZnONWs, the growth time was varied. A series of glass-ITO substrates containing ZnONWs were prepared at different times by fixing the following parameters: deposition of the seed layer by spin-coating with a thickness close to 10 nm,[53−55,57−60] temperature at 90 °C,[53−55,58,59] concentrations of $[Zn(NO_3)_2] = [HMTA] = 25$ mM,[56] reaction in an autoclave, and a medium volume of 15 mL. All the synthesis procedures under the chosen conditions resulted in controlled and reproducible nanowire growth. The morphologies of ZnONWs obtained as a function of growth time were characterized by scanning electron microscopy (SEM) analyses on the surface (*XY* plan) and on the cross section (*Z* direction). Representative photographs are shown in Figure 1.

Qualitatively, it was observed that 75 min is the minimum time required to initiate and activate the growth of the ZnONWs. A shorter duration did not lead to organized and dense ZnONW. The morphology of the nano-object appeared to be essentially controlled by the growth duration. All the parameters relevant for the application (areal number density, length, diameter, and inter-ZnONW distance) depend on the growth time. The morphological properties were thus quantified by dedicated image treatment and plotted against various durations. The results are presented in Figure 1. The ZnONWs experience a gradual and controlled evolution of their morphology. It is especially striking to note that two qualitatively different regimes are evidenced, which could be referred to as "short" and "long" growth time.

The quantitative analysis shows a regular evolution in the length of the ZnONW from 180 ± 50 nm (75 min) to about 2900 ± 100 nm (25 h) (brown curve in Figure 1). This large but monitored variation in the size follows two distinctive regimes roughly corresponding to the nanometer (blue area in Figure 1b, $t < 5$ h) and micrometer (red area in Figure 1b, $t > 5$ h) scales. On the kinetics standpoint, the growth of ZnONWs could actually be divided into three subregimes. The nanometric growth is divided into two steps with 74 ± 4

https://doi.org/10.1021/acsomega.1c01654
ACS Omega 2021, 6, 32365−32378

nm/h in [1.5, 3 h] and 980 ± 7 nm/h in [3, 5 h]. At the micrometer scale, a single and relatively slow regime was defined at about 59 ± 9 nm/h in [5, 25 h].

The average diameter of the ZnONW also presents two distinctive behaviors (orange curve in Figure 1). It first varies significantly during the first regime of growth corresponding to the nanometric scale. The diameter exhibits a minimum value of 22 ± 2 nm after 1 h 30 min and increases linearly with 4.3 ± 0.3 nm/h to reach a maximum diameter of 38 ± 3 nm after 5 h. In the second regime [5, 25 h], the growth rate is 2.5 times slower (1.7 ± 0.2 nm/h), and the diameter reaches a maximum of 75 ± 4 nm after 25 h.

The areal number density of ZnONWs also varies in two dissimilar regimes as a function of the reaction time (gray curve in Figure 1). In [1 h 30, 5 h], the particle number changes from 62 ± 5 ZnONW/μm^2 for 1 h 30 to 45 ± 5 ZnONW/μm^2 for 5 h. Within [5, 25 h], the number of ZnONW/μm^2 varies from 45 ± 5 ZnONW/μm^2 to 20 ± 3 ZnONW/μm^2. This variation might seem surprising at a first glance. One could argue that the number of ZnONW per unit area should originate from the precursor, and therefore remain quasiconstant over time. The two regimes evidenced here result from the SEM quantification method. The number of ZnONWs was determined from the number of those which significantly crosses through the seed layer to reach the top surface with apparent extremities. All the nonvertical, entangled ZnONWs and nonapparent ZnONWs owing to incomplete growth are not taken into account. As a result, the overall number of the crossing ZnONWs tends to decrease over time. Only counting the ZnONW crossing the layer seems reasonable for the application standpoint.

To assess the homogeneity of the vertical and radial growth of ZnONWs, the evolution of the aspect ratio (length/diameter) as a function of growth time was derived. As shown in Figure 1 (green curve), two regimes are identified again. The first regime of [1 h 30, 5 h], where a preferential anisotropic growth at 19 ± 3 nm/h along the c axis is observed. The second regime of [5, 25 h], where a less-anisotropic growth with 0.6 ± 0.2 nm/h is observed.

2.1.1. Mechanism of ZnONW Growth. The growth reaction of ZnONWs is a thermally activated reaction, considered to start at about 60 °C.[53] The kinetics of this reaction yet depends on several parameters such as pressure,[61] temperature,[53−55,58,59] pH,[62,63] agitation,[64] the amount of reagent/substrate interface,[65] the presence of a catalyst,[62] and concentration of the reagents during the course of the reaction.[66] Although we chose to maintain the reaction parameters as constant as possible to study the sole effect of time, the chemical reaction itself alters the different factors over time. The two very different growth rates identified from the morphological properties could, therefore, originate due to physical and/or chemical reasons. The reaction rate decrease as the reaction progresses could for instance originate from the depletion of the precursor inducing the long duration behavior. Another chemical effect could occur, with the presence of competitive secondary reactions leading to byproducts (screen effect). Physically, the presence of two regimes could suggest a limitation in the material transport and diffusion between the reaction medium and the ZnONW surface. A simple quantitative analysis furnished answers to these questions.

First, the depletion of the reaction medium in the precursor could be excluded by comparing the initial quantities of Zn^{2+} introduced to those involved in the growth reaction. Even for the longest reaction times, only 10^{-2} ppm of Zn^{2+} was converted into ZnONWs. The evolution of the Zn^{2+} ion concentration was thus disregarded as an influent parameter controlling the kinetics of the growth reaction.

To better understand the growth mechanism of the ZnONW and test the other hypotheses (diffusion of the precursors/surface reaction), several experimental models have been proposed in the literature. Coltrin et al.[67] performed a quantitative study of the growth of ZnONW. They used the specific areas of a patterned substrate with various sizes containing exposed and unexposed areas to the reaction medium and came up with a new understanding of the reactions rates. Their two-dimensional model accounts for the three successive mechanisms: the adsorption of the precursor at the surface, the actual chemical reaction with the nanowire, and the desorption of the reaction byproducts. This model reveals that the growth of ZnONWs depends on the size of the exposed surfaces. Increasing the amount of interface favors the vertical growth rate and the areal number density. This result was further confirmed by Boercker et al.,[65] who also attributed this difference to a gradient in the precursor's concentration in the vicinity of the substrate. The precursor's diffusion from the reaction medium to the substrate rationalizes the opposite trend between the length and diameter of the ZnONWs and their areal number density. This hypothesis was then validated by the calculation of the Thiele modulus, corresponding to the ratio between the reaction and diffusion rates. The Thiele modulus is given by eq 1[65]

$$(\Phi) = \left(\frac{N(k_Z \pi {R_w}^2) + (2k_r \pi R_w h\delta)}{D} \right) \quad (1)$$

where N is the areal number density of ZnONWs, D is the diffusion coefficient of Zn^{2+} in water ($D = 2.91 \times 10^{-5}$ cm^2/s[65]), δ represents the diffusion length of the precursors ($\delta \approx 3$ mm) estimated from the growth profile of the ZnONW according to the position,[65] R_w (cm) is the diameter of the nanowire, h is the length of the ZnO nanowire, k_Z (cm/min) is the vertical growth rate constant = length of a ZnONW in cm per growth time, and k_r (cm/min) is the lateral growth rate constant = diameter of a ZnONW in cm per growth time.

The Thiele modulus indicates the limiting factor in the chemical reaction. If $\Phi \ll 1$, it is the reaction at the surface of the ZnONW, whereas if $\Phi \gg >1$ it is the diffusion to the surface.[65] This model has been validated experimentally several times in the literature. It was directly applied in the current work. The Thiele modulus Φ was calculated as a function of the reaction time, Figure 2. Under all tested conditions, the Thiele modulus remains significantly larger than the critical value of 1. In the studied systems, the growth is thus limited by the diffusion of the precursors to the surface. This was also the case in prior works with similar systems.[65,67] The Φ values remained somewhat constant during both nanometric and micrometric growth, indicating a similar mechanism regardless of the scale. Nevertheless, the Φ value shows a significant change around the transition between the two regimes. This was attributed to the presence of the dual scale (nano/micro) ZnONW with a different diffusion combinatorial mechanism during the growth reaction.

2.2. Application of ZnONWs in PV Solar Cells. For an optimal integration in PV application, a target morphology has been predesigned depending on the critical exciton diffusion length and the charge carrier transport distances in organic AL

https://doi.org/10.1021/acsomega.1c01654
ACS Omega 2021, 6, 32365−32378

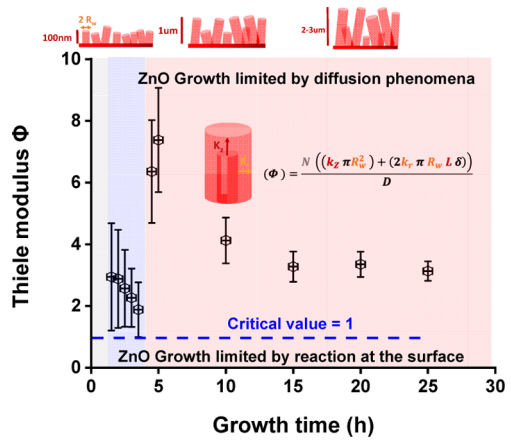

Figure 2. Thiele's modulus Φ as a function of growth time.

and ZnO. The ideal architecture is presented in Scheme 1. This morphology corresponds to an average length of 200 nm,[68] an average diameter of around 30 nm, and an average internanowire distance of around 100 nm. These dimensions were defined as a good compromise between solar cell processability, synthesis reproducibility, and the critical distance of exciton diffusion and carrier charge transport.[69] Many synthesis batches were performed under the best conditions to obtain the target dimensions. The reproducibility was thereby confirmed, and the numerous substrates could be used to further optimize the integration of the ZnONW array as an electron transport layer in a functional PV cell.

2.2.1. Optimization of Devices. The development of solar cell devices is a challenging road. They should combine many high-quality functional materials integrated with good interfaces in the structure (Scheme 1). The final product contains many nano-sized layers (AL, HTL, anode). In the present case, it should additionally be deposited on a rough ZnO surface, and the cavities between ZnONWs should be filled properly. Finally, the large interfaces created to gather more current during the PV process should also be of quality. This concept was first tested with the photoactive materials on a conventional ZnO layer (flat, 2D). The process was then extended to the ZnONW network with a progressive increase in the roughness of ZnO and its corresponding specific surface. Several methods have been tested to obtain satisfactory results.

The nanometric size and roughness of the ZnONW network primarily control the deposition method, and the optimal process differs largely from the best counterpart, regular 2D devices. The initial adjustments of the processing parameters essentially followed a trial and error method. This could, however, eventually lead to a fair understanding of the mechanisms monitoring the AL deposition. Three dissimilar flaws could be identified with the qualitative analysis of the SEM pictures Figure 3: (a) the incomplete diffusion of the AL, leading to hollow structures, with voids near the ZnO seed layer and (b) the insufficient of control of the AL thickness. It may be too thin, leading to shortcuts (not presented in Figure 3) or too thick inducing a loss of charge carrier, and (c) the poor control of the surface roughness. A coarse surface at the micron scale prohibits the realization of functional devices. To ensure a complete and controlled impregnation of ZnONWs with the AL (Figure 3d), four different deposition methods were tested, as described in Figure 3.

The spin-coating at room temperature systematically resulted in imperfect arrangements. Changing the time or rotational speed proved ineffective to improve the deposition. In contrast, varying the pressure in the environment (large pressure or vacuum) on the AL solution favors the impregnation of the ZnONW. The repetitive application of high and low pressure on the structure also helps the air removal and favors impregnation. This probably results from the limited diffusion of air both in and out when trapped in a confined environment between the ZnONW layer and the AL. Pressure changes push the solution to fill the air pockets between the ZnONWs. This procedure does, however, not allow us to properly control the thickness and the roughness of the upper layer. The extremely thin layers utilized to complete the devices (in the nm range) may not accommodate such large differences in the height. The best processing alternative consists in high-temperature spin-coating. This process reduces the viscosity of the solution with a relatively high temperature (100 °C), enabling the diffusion in the tiny pores. The increase of temperature may also alter the surface tension of the solution to promote the wetting on the ZnONW. Finally, a high rotational speed of the coater favors the conformal deposition and removes the extra solution. After a proper optimization, samples could be obtained in a reproducible manner with a stacking close to the ideal target, Figure 3d′. The ZnONW network is completely covered by the AL, with a thickness close to the ideal target.

In addition to the morphological control of the deposited AL, its direct influence on the solar cell performances was determined independently and compared. Global setups were

Scheme 1. Morphological Characteristics and Dimensions of an Ideal ZnONW Network for an Optimal Solar Cell Assembly: ZnONW Length ≈200 nm, ZnONW Diameter ≈30 nm, and Inter-ZnONW Distance ≈100 nm (Left), and Cross Section (Right), *XY* Plan

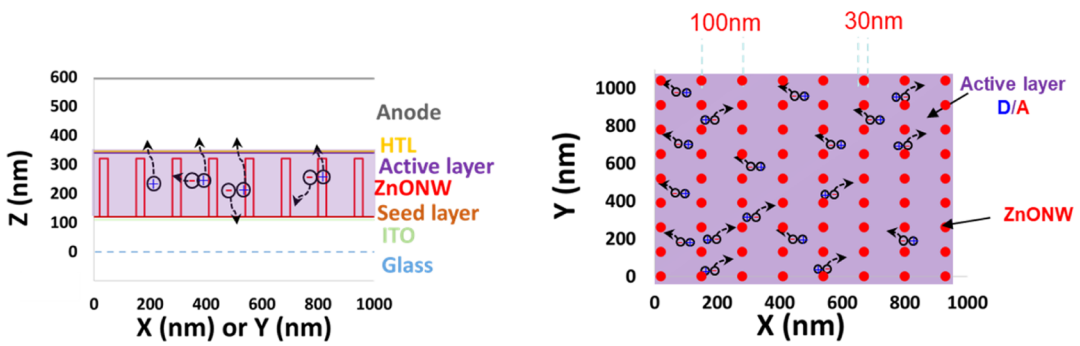

https://doi.org/10.1021/acsomega.1c01654
ACS Omega 2021, 6, 32365−32378

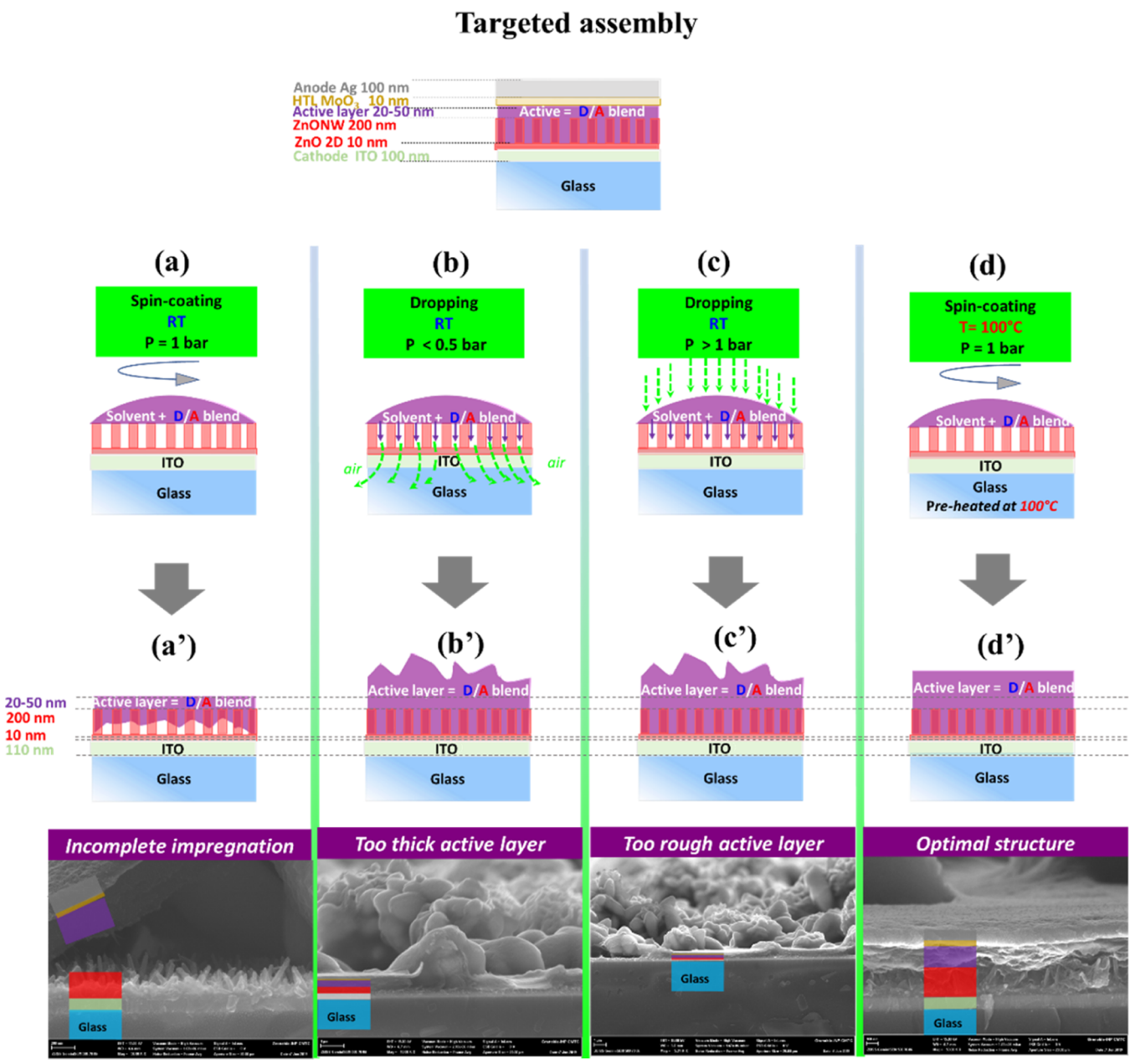

Figure 3. Ideal assembly (on top), thickness of AL of 200 nm, complete impregnation in the ZnONW, and the upper additional layer ~20 to 50 nm to prevent shorts. Different methods tested for the deposition of the AL on the ZnONW: (a) spin-coating at room temperature, (b) vacuum immersion impregnation, (c) pressurized impregnation after immersion, and (d) high-temperature spin-coating. Typical SEM images and schematic illustration of the different setups after deposition, (a′) incomplete impregnation, hollow spaces on the bottom, (b′) too thick AL (≫250 nm), (c′) too rough AL, and (d′) optimal structure.

prepared using the optimized ZnO nanowire substrates. The chemical composition of the AL was also kept constant to favor the comparison (PBDD4T-2F:$PC_{71}BM$, 1:0.9). The solutions were prepared with 15 g/L chlorobenzene. Figure 4 presents the $J-V$ curves obtained with the most efficient PV cells to compare the four deposition techniques described in Figure 3. All cells exhibit a clear PV effect, but the outcomes strongly vary from one method to another.

First, the cells prepared by immersion with either low or high pressure led to comparable low performances with a PV conversion efficiency (PCE) of 0.09 and 0.12%, respectively (Table 1). This indicates that the control of the layer thickness is vital to process functional cells. PV cells made using vacuum immersion have a short-circuit current density (J_{sc}) of 5.27 mA/cm^2, an open-circuit voltage (V_{oc}) of 0.08 V, and a fill factor (FF) of 23%, resulting in a PCE of 0.09%. The high-pressure counterpart seems slightly better, but remains very low. They have a short-circuit current density J_{sc} of 1.57 mA/cm^2, a V_{oc} of 0.3 V, an FF of 26%, and a PCE of 0.12% (Table 1). The two systems could hardly qualify as PV cells and these structures were disregarded for the rest of the study.

In contrast, the spin-coated cells produced well-defined $J-V$ curves, in all cases at room or high temperature. Substantial PCEs of 1.3 and 2.05% were obtained. The optimal assembly led to a J_{sc} of 11.87 mA/cm^2, combined with a V_{oc} of 0.54 V and a FF of 32%. The PCE characterization thus confirmed the morphological analysis. The high-temperature spin-coating combines the desirable properties of impregnation of the

https://doi.org/10.1021/acsomega.1c01654
ACS Omega 2021, 6, 32365−32378

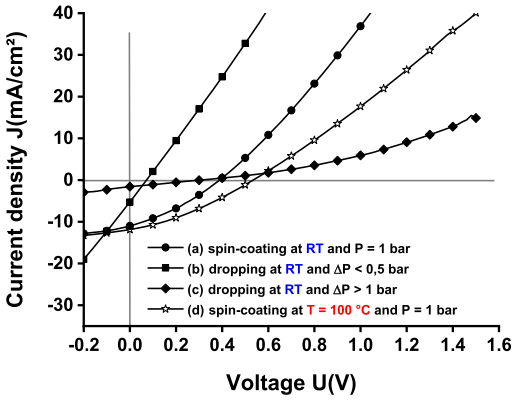

Figure 4. $J-V$ characteristics under illumination (AM1.5 standard) of PV cells based on ALs of PBDD4T-2F:$PC_{71}BM$ 1: 0.9 (solution at 15 g/L in chlorobenzene). Influence of the processing conditions on the performance. (a) Spin-coating at room temperature, dropping immersion with (b) low and (c) high pressure, and (d) and hot spin-coating.

ZnONW, control of the thickness of the AL, and the robustness of the processing. At this stage, the processing protocol was settled, and the D/A ratio could be varied to maximize the overall performances. In particular, it seemed to be reasonable to improve V_{oc} and parallel resistance (R_p) with the proper changes in the AL and its interfaces.

2.2.2. D/A Ratio of Photoactive Materials. The optimizations had so far been based on AL with a D/A ratio of 1:0.9. This is, however, a key factor to optimize the cell efficiency and durability.[70] The PCE can be improved either by adapting the D/A ratio for an optimal functional properties, including absorption and transport properties, and optimal morphology with D/A arrangement, which maximize the D/A interface while ensuring homogeneous and continuous domains.[69,71−73] A ratio of 1:1 is generally considered as close to the optimal D/A in organic cells. It has, however, been found to vary for instance with the chemistry of the polymers or its average molecular weight.[74,75] Under some circumstances, a comprehensive understanding of the optimal ratio has been proposed. High-molecular-weight polymers tend to incorporate the $PC_{71}BM$ and prevent the formation of the continuous acceptor domains.[76,77] The latter should, therefore, be placed in a larger percentage for a better controlled phase separation and for triggering the PV effect.[75] The optimal D/A ratio also depends on the processing steps of the AL that control the size distribution of the D/A phases.[75,77]

To obtain the optimal D/A composition, similar solar cells were processed with various PBDD4T-2F:$PC_{71}BM$ ratios ranging from 0.5 to 2. All the other parameters were kept constant, especially the thickness of the AL close to 200−250 nm. Figure 5 shows the $J-V$ curves of the cells produced and Table 2 summarizes the PV performances obtained. PV

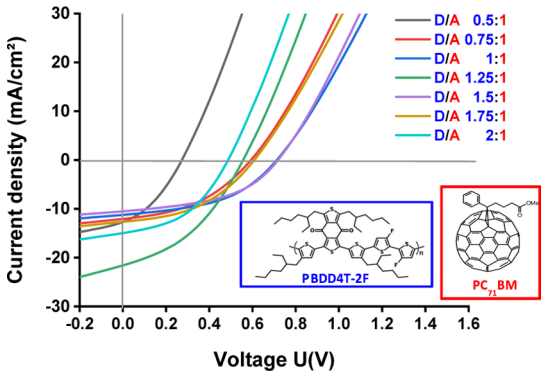

Figure 5. $J-V$ characteristics under illumination of the best PV cells with various D/A ratios.

performances varied significantly with the D/A ratio. The structural parameters that control the changes remained hard to establish, but the PV cells with a D/A ratio of 1.25:1 presented the best performance of both J_{sc} and PCE.

Figure 6 shows the large effect of the PBDD4T-2F:$PC_{71}BM$ ratio on the PV performances. The PV parameters do not seem to vary gradually with D/A and a nonmonotonic behavior is observed. This may result from a complex balance between the composition, the position of solar cell on the substrate (one substrate contains six individual cells) and processing conditions, or from the presence of sensitive parameters hard to detect. For this reason, the individual results have been presented in the graph. The overall trend shows a maximum PCE for the ratio of 1.25:1 of PBDD4T-2F:$PC_{71}BM$.

The presence of residual traces of solvents or additives can have a negative effect on PV performances.[78] At room temperature and atmospheric pressure, these traces cannot be completely removed. Several methods are used in the literature such as vacuum/thermal postannealing, or washing with an inert solvent such as methanol[79,80] or isopropanol.[81] These post-treatments can also lead to a significant improvement in the morphology of the AL. In this study, the methanol wash was tested before and after the deposition of the AL, following this scheme: (i) washing the substrate with methanol before depositing the AL and (ii) washing the substrate with methanol before deposition of the AL and washing the AL after deposition. (iii) Washing the AL with methanol after deposition. Figure 7 shows the $J-V$ characteristics of ZnO-2D- and ZnO-3D-based solar cells with three methanol pre/post-treatments. Table 3 summarizes the PV performances obtained for each treatment and for the two 2D and 3D structures. The results show that for both 2D and 3D structures, V_{oc} is almost

Table 1. PV Cells Based on ALs of PBDD4T-2F:$PC_{71}BM$ 1:0.9 (in Chlorobenzene as a Solvent and at a Concentration of 15 g/L) Produced with Different Deposition Methods: (a) Spin-Coating at Room Temperature, Dropping Immersion with (b) Low and (c) High Pressure, and (d) and Hot Spin-Coating[a]

method of AL deposition	J_{sc} (mA/cm²)	V_{oc} (V)	FF (%)	PCE (%)	EQE (%)	R_s (Ω cm²)	R_p (Ω cm²)
(a) spin-coating at RT and P = 1 atm	11	0.38	33	1.3	15.9	14	94
(b) dropping at RT and ΔP < 0.5 bar	5.27	0.08	23	0.09	7.6	11	14
(c) dropping at RT and ΔP > 1 bar	1.57	0.3	26	0.12	2.3	63	196
(d) spin-coating at T = 100 °C and P = 1 bar	11.87	0.54	32	2.05	17.2	23	112

[a]EQE: External quantum efficiency, R_p: parallel resistance, and R_s: series resistance.

https://doi.org/10.1021/acsomega.1c01654
ACS Omega 2021, 6, 32365−32378

Table 2. PV Performance of the Best PV Cells Based on ALs for Various D/A Ratios[a]

AL D/A	D/A ratio	J_{sc} (mA/cm^2)	V_{oc} (V)	FF (%)	PCE (%)	EQE (%)	R_s (Ω cm^2)	R_p (Ω cm^2)
PBDD4T-2F/$PC_{71}BM$	0.5/1	12.7	0.28	34	1.22	18.4	7	35
	0.75/1	12.1	0.60	42	3.01	17.5	10	155
	1/1	11.2	0.72	46	3.70	16.2	12	237
	1.25/1	21.6	0.56	39	4.70	31.3	7	61
	1.5/1	10.5	0.72	47	3.53	15.2	11	247
	1.75/1	12.7	0.6	44	3.36	18.4	12	166
	2/1	15.0	0.48	45	3.21	21.7	8	93

[a]EQE: External quantum efficiency, R_p: parallel resistance, and R_s: series resistance.

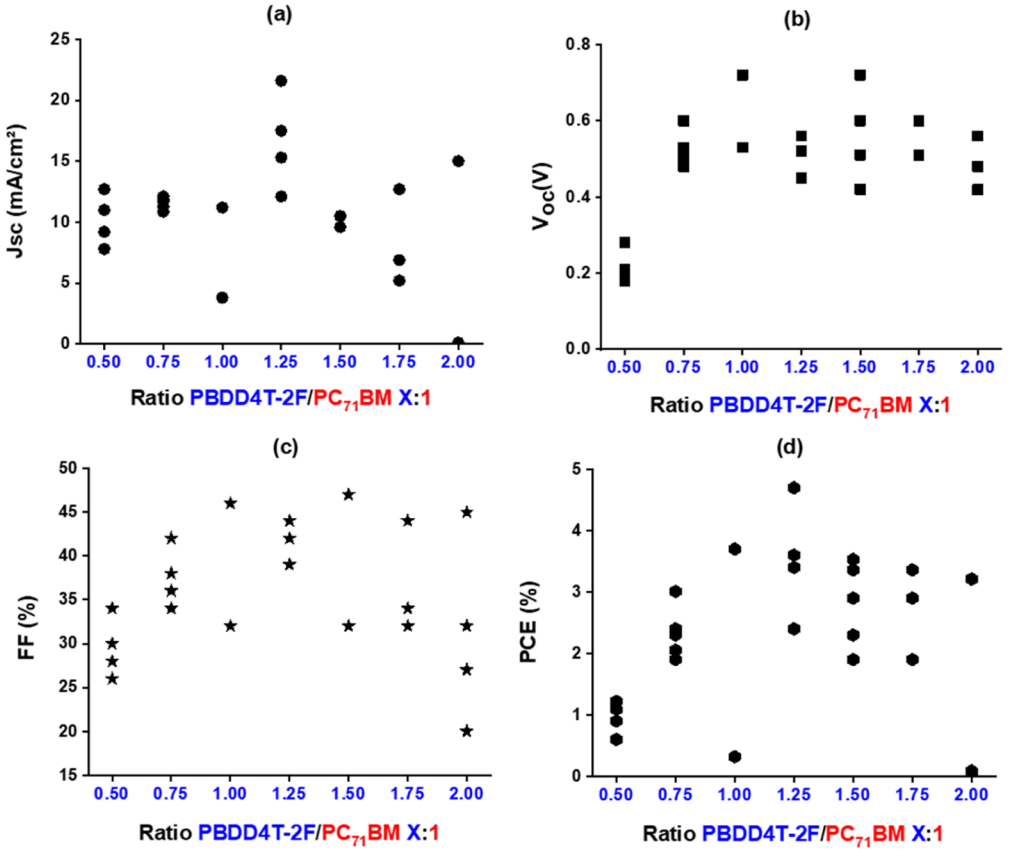

Figure 6. PV Performances of PV solar cells for various D/A ratios, (a) short-circuit current density (J_{sc}), (b) open-circuit voltage (V_{oc}), (c) FF, and (d) PCE.

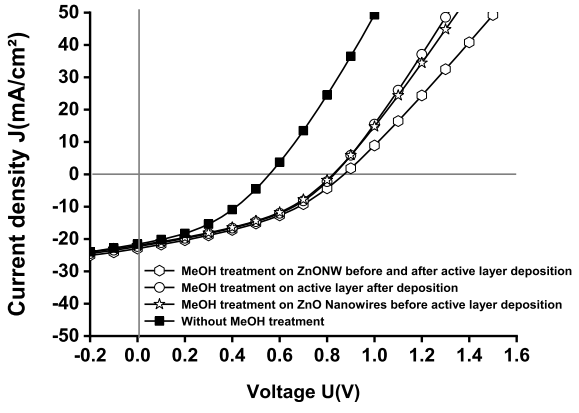

Figure 7. $J-V$ characteristics of solar cells based on AL of PBDD4T-2F:$PC_{71}BM$ 1.25:1 and an ETL of ZnONW. Influence of the methanol pre/post-treatments.

identical but with a very slight variation depending on the washing method. J_{sc} varies slightly from the three cases. The increase in current by washing the substrate and the AL with methanol can be explained by the improvement of the wettability between the solution of the AL and the surface of ZnONW, and the generation of a greater number of charges thanks to the reduction in the recombination phenomena at the improved interfaces between the hydrophobic AL and the ETL(ZnO) and HTL(MoO_3) interfacial layers.

2.2.3. Effect of the ZnO Nanostructure on PV Performances: ZnO-2D (Planar Structure) versus ZnO-3D (ZnONW). A 3D nano-textured architecture has several advantages compared to a 2D planar structure for PV applications.[14,44,82] It favors the photon trapping and thus improves the absorption process, and it increases the surface of interface for light–matter interaction and charge collection.[83,84] As a result, a larger area between the AL and the ETL is expected to significantly improve the overall PCE.

https://doi.org/10.1021/acsomega.1c01654
ACS Omega 2021, 6, 32365−32378

Table 3. PV Performance of Solar Cells Based on AL of PBDD4T-2F:$PC_{71}BM$ 1.25:1 and an ETL of ZnONW (EQE: External Quantum Efficiency, R_p: Parallel Resistance, and R_s: Series Resistance)

AL D/A	ratio D/A	treatment	J_{sc} (mA/cm^2)	V_{oc} (V)	FF (%)	PCE (%)	EQE (%)	R_s (Ω cm^2)	R_p (Ω cm^2)
PBDD4T-2F/$PC_{71}BM$ ETL = ZnONW	1.25/1	- without post-treatment	21.6	0.56	39	4.7	31.3	7	61
		- MeOH treatment on ZnONWs before and after AL deposition	22.9	0.88	38	7.72	33.2	13	85
		- MeOH treatment on AL after deposition	22.4	0.84	39	7.40	32.5	9	85
		- MeOH treatment on ZnONWs before AL deposition	22.0	0.82	40	7.27	31.9	10	88

UV−visible transmission was evaluated on 2D- and 3D-ZnO layers with and without AL. No effect of nanostructuration could be identified with the AL, because of its large absorption compared to the transparent ZnO. In contrast, significant differences were observed between the neat ZnO layers. The photon−ZnO interactions are altered by the nanostructuration,[85,86] the absorption edge increases from 300 to 380 nm and optical interference fringes appear (Figure 8).

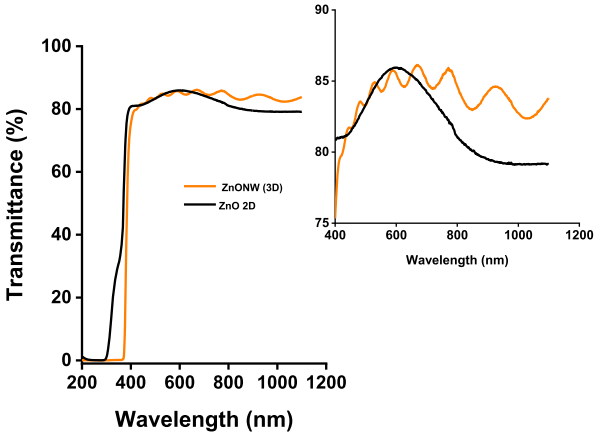

Figure 8. UV−visible transmission spectra of the ZnO planar layer (black) and the ZnONW layer (orange), left: whole spectra; right: detailed view.

Figure 9 shows the $J-V$ curves of the optimized cells made with an AL PBDD4T-2F:$PC_{71}BM$ 1.25:1 and the two ZnO nanostructures (2D planar and 3D ZnONW). The PV performances of these cells are shown in Table 4. The cell in the 2D structure generated a J_{sc} of 12.5 mA/cm^2, a V_{oc} of 0.92 V, a FF of 49%, which resulted in an efficiency of 5.63%. PV cells based on ZnONWs have a J_{sc} of 22.9 mA/cm^2, a V_{oc} of 0.88 V, an FF of 38%, inducing an efficiency of 7.72%.

The beneficial effect of transport layer structuration on the cell performance has already been identified in the literature. In organic solar cells, Ho et al.[87] demonstrated that increasing the specific surface of an ETL increased the PCE. They suggested that ZnONWs act as electron transport nanochannels and reduce the electron−hole recombination in the AL. The PCE of PBDTTT-C-T/$PC_{71}BM$-based solar cells improved from 5.4 to 7.3%, with the nanostructuration. Similar results have been shown with inorganic cells. Majidi et al.[88] demonstrated that the use of CdSe−ZnONW doubled J_{sc} (from 3.3 to 6.6 mA/cm^2), but reduced both V_{oc} (0.62 to 0.52 V) and FF (50 to 39%). Overall, the PCE improved from 1.03 to 1.34% compared to ZnO-2D.

The comparison between 3D ZnONW cells and 2D planar cells shows comparable V_{oc}. This value was not expected to vary when changing the geometrical features of the cell[69,89,90] because it mainly depends on the chemical nature of the materials and the alignment of their energy levels.[89,90] In contrast, J_{sc} was found to double. This remarkable result should solely be ascribed to the photon absorption[84] and carrier charge collection,[87] that is, to the large specific surface of the cells structured with ZnONWs (estimated to be 6.6 $\mu m^2/\mu m^2$) compared to planar cells. This result also suggests that the main limitation of the initial setup was on the ETL

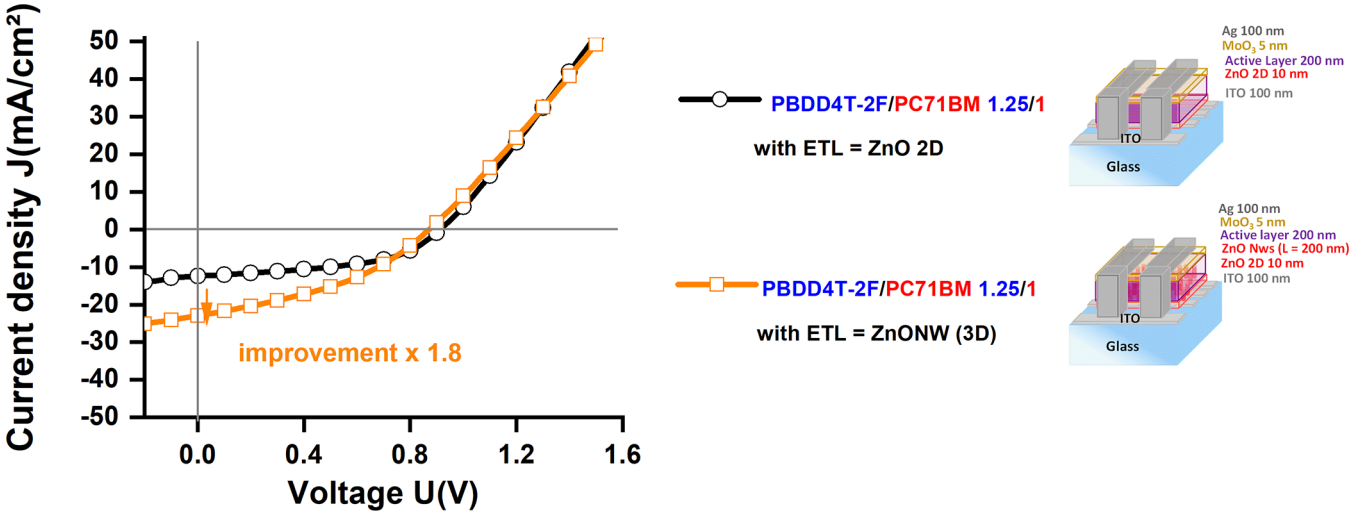

Figure 9. $J-V$ curve under illumination of the best PV cells based on the ZnO planar layer (○) and the ZnONW layer (□).

https://doi.org/10.1021/acsomega.1c01654
ACS Omega 2021, 6, 32365−32378

Table 4. Comparison of PV Performance of PV Cells Based on AL of PBDD4T-2F:$PC_{71}BM$ 1.25:1, with ETL Being Either a 2D ZnO Layer or a 3D ZnONW Network[a]

architecture	$\mu m^2/\mu m^2$	post-treatment	J_{sc} (mA/cm^2)	V_{oc} (V)	FF (%)	PCE (%)	EQE (%)	R_s (Ω cm^2)	R_p (Ω cm^2)
2D	1	MeOH treatment on ZnONWs before and after AL deposition	11	0.92	49	5.63	16	11	146
3D	6.6		22.9	0.88	38	7.72	33.2	13	85

[a]EQE: External quantum efficiency, R_p: parallel resistance, and R_s: series resistance.

side of the AL. In addition, the cells with ZnONWs presented a lower FF than the 2D-ZnO counterpart. This mainly results from the increase in the series resistance due to the lower interface quality between the ZnONWs and AL. This critical interface could much more be affected by the wettability problems.[91] This problem should be addressed for future developments of 3D cells.

3. CONCLUSIONS

We showed the successful synthesis of customized ZnONWs by an improvement of the hydrothermal method previously described in the literature. An optimization of the process permitted to develop the ideal structure for application in solar cells, with much shorter ZnONWs on a millimeter-/centimeter-scale surface. This was achieved with the continuous measurement of the length of ZnONWs. The growth rate follows qualitatively two different regimes, interestingly separating the nanometer and micrometer scales in the wire's length. The optimal longitudinal growth in the 001 direction and at the nanometric scale could thus be obtained after a relatively short reaction time (102 ± 14 min) to reach an optimal length of about 200 ± 30 nm.

The calculation of the Thiele modulus (Φ) as a function of time revealed that the diffusion of the reagents primarily governs the growth mechanism. The ratio between the reaction and the diffusion rates remained larger than one during the entire course of the synthesis. Φ was almost constant throughout the process, except at the nm−μm transition, where the experimental data showed a larger dispersion. The uncertainty of Φ at the transition between the two regimes was attributed to the presence of the dual scale (nano/micro) ZnONW with a different diffusion combinatorial mechanism.

For PV applications, there is also a need to control the areal number density of ZnONWs, around 60 ZnONW/um^2 and a diameter close to 30 nm. The controlled synthesis led to an internanowire distance of 100 nm, close to the target. These morphological characteristics allow a good compromise between processability of the solar cells and critical distances of exciton diffusion and carrier charge transport properties.

For application in solar cells, PBDD4T-2F and $PC_{71}BM$ were chosen as donor (D) and acceptor (A) materials. The optimization of ambient air-processed solar cells based on ZnONWs required the development of an unusual assembly method. The regular spin-coating was performed here at 100 °C to favor the diffusion and impregnation process.

The D/A ratio and the pre/post-treatments were also varied to maximize the performances. The best device so far was the one with a D/A ratio of 1.25/1, and methanol treated on ZnONWs before and after the deposition of AL. Improved performances were obtained for solar cells based on the ZnONW architecture, with a short-circuit current density close to 22 mA/cm^2 (2 times better than that of the 2D-ZnO cells), and the power conversion efficiency close to 7.7% (1.4 times better than that of 2D-ZnO cells).

This improvement with the 3D architecture results from the increase in the specific surface area (ZnO/AL) from 1 $\mu m^2/\mu m^2$ for the 2D structure to 6.6 $\mu m^2/\mu m^2$ for the 3D architecture, and the presence of ZnONWs within the AL to collect the electrons (~60 ZnONW/μm^2). It also indicates that the main limitation in the initial system was on the ETL side of the setup. These results validate the concept of nanotexturing the substrates to develop efficient cells. It could now be further improved and developed with other efficient and more stable ALs.

4. EXPERIMENTAL SECTION

4.1. Synthesis of ZnONWs. Aqueous solutions of zinc nitrate hexahydrate ($Zn(NO_3)_2{\cdot}6H_2O$) and HMTA at a fixed concentration (25 mmol/L) were prepared and stirred for a few minutes until the complete dissolution. A reaction medium is prepared by mixing 7.5 mL of each solution. This solution is transferred to an autoclave with a total capacity of 50 mL (supplied by Techinstro). For the hydrothermal growth of ZnONWs, precleaned commercial glass/ITO substrates were used. First, 10 nm of a seed layer based on ZnO was deposited by spin-coating (22 rps/3 s/45 s) using a commercial (Aldrich) suspension of 2.5 wt % of ZnO nanoparticles (8−16 nm) in an isopropanol/propylene glycol diluent and with a viscosity of 3 cP. The substrate is dried on a hot plate at 90 °C for 10 min. The quality of the seed layer is controlled at different scales and the substrate is exposed to the reaction medium by flotation. The optimal configuration of glass up and the ITO/seed layer down for contact with the solution was chosen to avoid undesirable deposits by precipitation of the reagents, products, and byproducts on the surface of the substrate. Finally, the autoclave is placed in an oven at 90 °C to grow the ZnONW. The duration is varied from 30 min to 25 h. After each growth process, the substrate is rinsed with distilled water and the resulting morphology is characterized qualitatively and quantitatively.

4.2. Morphological Characterization. The morphology of each ZnONW batch was characterized with a scanning electron microscope (MEB-FEG Zeiss Gemini SEM 500). The results are presented as 16-bit images with an indication of the scale. The quantifications of morphological properties were carried out by ImageJ software on several photographs either of the same sample in different zones, or of several samples prepared under identical conditions.

4.3. Solar Cell Assembly and Characterization. *4.3.1. Substrate Preparation.* Commercial glass/ITO substrates have been purchased from Ossila. The ITO layer consists of a mixture of 90 wt % indium oxide In_2O_3 and 10 wt % tin oxide SnO_2. The dimensions of the substrates are 20 mm × 15 mm × 1.1 mm. The substrates contain six individual ITO electrodes with a roughness of 1.8 nm rms, a thickness of 100

https://doi.org/10.1021/acsomega.1c01654
ACS Omega 2021, 6, 32365−32378

nm, and an area of 6 $mm^2 \approx 4$ mm × 1.5 mm each. The surface electrical resistance of ITO is 20 Ω/sq and the visible transmittance is around 85 to 90%. These substrates were cleaned before the synthesis of ZnONWs, and used for the production of 2D and 3D solar cells. ITO/glass substrates were sonicated in deionized water for 5 min and rinsed thoroughly with deionized water, resonicated in several solvents (acetone, ethanol, and isopropanol) for 5 min, and rinsed after each sonication cycle, before to be dried at 60 °C for 20 min. ITO-patterned glasses are then exposed to UV-O_3 treatment (Ossila UV ozone cleaner E511) for 30 min.

4.3.2. Preparation of the AL Solution. The AL (AL) is prepared using the commercial donor PBDD4T-2F polymer purchased from Ossila (138 kg/mol, PDI = 2.6) and acceptor $PC_{71}BM$ from Solarmer (purity 99%). Powder of $PC_{70}BM$ and meshes of PBDD4T-2F were weighed using a Mettler-Toledo balance (10^{-2} mg precision). The AL solutions were elaborated under ambient air using anhydrous chlorobenzene as a solvent with a total concentration of 15 g/L for PBDD4T-2F/$PC_{71}BM$ blends, first with a ratio of 1/0.9 for the processing method selection and other various ratios for the optimization of the AL. The so-prepared solutions were stirred at 80 °C for 2 h before deposition on glass/ITO/ETL substrates.

4.3.3. Deposition of AL for 2D Solar Cells. The 2D configuration was prepared with: glass/ITO (cathode)/ZnO/AL/hole transport layer (HTL)/Ag (anode). Commercial suspension of 2.5 wt % of ZnO nanoparticles (8−16 nm) in the isopropanol/propylene glycol diluent and with a viscosity of 3 cP is purchased from Aldrich. A very thin layer of ZnO (10 nm) was deposited as ETL by spin-coating (22 rps/3 s/45 s) on glass/ITO substrates, followed by drying on a hot plate at 90 °C for 10 min. The substrate glass/ITO/ZnO and the plate of the spin-coater were preheated on a hot plate at 100 °C 5 min before deposition. Then, the hot AL solution (80 °C) was deposited by spin-coating at 22 rps/3 s/45 s.

The assembly of solar cell was completed by deposition via thermal evaporation of around 5 nm of MoO_3 used as HTL and a silver-based 100 nm thick top anode. For HTL deposition, the chamber pressure was set to 10^{-6} mbar with a current intensity of 2.4−2.6 A and a voltage of 10 V for 10 s (deposition rate of ≈0.1 nm/s). Ag thermal evaporation was conducted with a pressure of 10^{-6} mbar, a current intensity of 3.8−4 A, and a voltage of 10 V for ≈40−60 s (deposition rate ≈2 nm/s) with a controlled overall thickness of 100 nm.

4.3.4. Deposition of AL 3D Solar Cells. For 3D solar cells, a configuration of glass/ITO (cathode)/ZnONW/AL/HTL/Ag (anode) was used. The impregnation of ZnO-NWs with AL was tested using four methods and conditions, that is, (i) conventional spin-coating at 22 rps/3 s/45 s at room temperature (ii) at 100 °C, (iii) vacuum dropping, and (iv) dropping under pressure. For spin-coating at 100 °C, the hot AL solution (80 °C) is deposited by spin-coating at 22 rps/3 s/45 s on the preheated (5 min at 100 °C) substrate and spin-coater plate. The vacuum dropping is carried out, at room temperature and 10^{-3} mbar for a few minutes using an home-made experimental device. Dropping under pressure is performed using an autoclave chamber equipped with a nitrogen supply allowing pressurization at room temperature with an overpressure of 1 bar.

4.3.5. Characterization of Solar Cell Performances. The PV performances were calculated using an AL surface of 4.5 mm^2 and from the current density−voltage ($J-V$) characteristics of the assembled solar cells. The $J-V$ characteristics were recorded under AM1.5 standard illumination (Oriel LCS-100 solar simulator, 100 mW/cm^2) using an Agilent B2902A Source Measure Unit calibrated with a silicon reference cell.

AUTHOR INFORMATION

Corresponding Author

Ali Nourdine − *Univ. Grenoble Alpes, Univ. Savoie Mont Blanc, CNRS, Grenoble INP, LEPMI, 38000 Grenoble, France;* orcid.org/0000-0003-2611-0788; Email: Ali.nourdine@univ-smb.fr

Authors

Marwen Abdelli − *Univ. Grenoble Alpes, Univ. Savoie Mont Blanc, CNRS, Grenoble INP, LEPMI, 38000 Grenoble, France*

Nicolas Charvin − *Univ. Grenoble Alpes, Univ. Savoie Mont Blanc, CNRS, Grenoble INP, LEPMI, 38000 Grenoble, France;* orcid.org/0000-0003-2696-0993

Lionel Flandin − *Univ. Grenoble Alpes, Univ. Savoie Mont Blanc, CNRS, Grenoble INP, LEPMI, 38000 Grenoble, France;* orcid.org/0000-0003-3582-7705

Complete contact information is available at: https://pubs.acs.org/10.1021/acsomega.1c01654

Notes

The authors declare no competing financial interest.

ACKNOWLEDGMENTS

This work was performed within the framework of the Center of Excellence of Multifunctional Architectured Materials (CEMAM), no. AN-10-LABEX-44-01 (Project Earth: Eco-friendly ARchitectured materials for photoassisted TecHnology). This work has been supported by the French National Research Agency, through Investments for Future Program (ref. ANR-18-EURE-0016 − Solar Academy). LEPMI laboratory is a member of the INES Solar Academy Research Center. The authors acknowledge CMTC (Consortium des Moyens Technologiques Communs) for the provision of the equipment/accessories required for the SEM analyses and Johann Ravaux for help on SEM characterization and fruitful discussions.

REFERENCES

(1) Berger, P. R.; Kim, M. Polymer solar cells: P3HT:PCBM and beyond. *J. Renewable Sustainable Energy* **2018**, *10*, 013508.

(2) Dang, M. T.; Hirsch, L.; Wantz, G. P3HT:PCBM, Best Seller in Polymer Photovoltaic Research. *Adv. Mater.* **2011**, *23*, 3597−3602.

(3) Li, W.; Zhang, S.; Zhang, H.; Hou, J. The investigations of two conjugated polymers that show distinctly different photovoltaic properties in polymer solar cells. *Org. Electron.* **2017**, *44*, 42−49.

(4) Medlej, H.; Nourdine, A.; Awada, H.; Abbas, M.; Dagron-Lartigau, C.; Wantz, G.; Flandin, L. Fluorinated benzothiadiazole-based low band gap copolymers to enhance open-circuit voltage and efficiency of polymer solar cells. *Eur. Polym. J.* **2014**, *59*, 25−35.

(5) El-Moussawi, Z.; Medlej, H.; Nourdine, A.; Berson, S.; Toufaily, J.; Hamieh, T.; Flandin, L. Development of Dithienosilole-Pyridalthiadiazole-Based Copolymer as an Electron Donor in Organic Photovoltaic Cells. *IEEE Trans. Nanotechnol.* **2017**, *16*, 574−581.

(6) Ganesamoorthy, R.; Sathiyan, G.; Sakthivel, P. Review: Fullerene based acceptors for efficient bulk heterojunction organic solar cell applications. *Sol. Energy Mater. Sol. Cells* **2017**, *161*, 102−148.

(7) Zhang, S.; Qin, Y.; Uddin, M. A.; Jang, B.; Zhao, W.; Liu, D.; Woo, H. Y.; Hou, J. A Fluorinated Polythiophene Derivative with

Stabilized Backbone Conformation for Highly Efficient Fullerene and Non-Fullerene Polymer Solar Cells. *Macromolecules* **2016**, *49*, 2993−3000.
(8) Nourdine, A.; Perrin, L.; Albérola, N.; Flandin, L. Extrusion as plausible processing method for production of organic photovoltaic solar cells *2014 IEEE 40th Photovoltaic Specialist Conference (PVSC), 8−13 June 2014*, 2014; pp 2581−2583.
(9) Nourdine, A.; Flandin, L.; Albérola, N.; Perrin, L.; Planès, E.; Hiltner, A.; Baer, E. Extrusion of a nano-ordered active layer for organic photovoltaic cells. *Sustainable Energy Fuels* **2017**, *1*, 2016−2027.
(10) Yang, Y.; Mielczarek, K.; Aryal, M.; Zakhidov, A.; Hu, W. Nanoimprinted Polymer Solar Cell. *ACS Nano* **2012**, *6*, 2877−2892.
(11) El-Moussawi, Z.; Nourdine, A.; Flandin, L. A key progress in introducing single walled carbon nanotubes to photovoltaic devices. *Appl. Nanosci.* **2020**, DOI: 10.1007/s13204-020-01561-1.
(12) Jiang, Y.; Shen, H.; Pu, T.; Zheng, C.; Tang, Q.; Gao, K.; Wu, J.; Rui, C.; Li, Y.; Liu, Y. High efficiency multi-crystalline silicon solar cell with inverted pyramid nanostructure. *Sol. Energy* **2017**, *142*, 91−96.
(13) Chen, C.; Jia, R.; Yue, H.; Li, H.; Liu, X.; Ye, T.; Kasai, S.; Tamotsu, H.; Wu, N.; Wang, S.; Chu, J.; Xu, B. Silicon nanostructure solar cells with excellent photon harvesting. *J. Vac. Sci. Technol., B: Nanotechnol. Microelectron.: Mater., Process., Meas., Phenom.* **2011**, *29*, 021014.
(14) Shinagawa, T.; Shibata, K.; Shimomura, O.; Chigane, M.; Nomura, R.; Izaki, M. Solution-processed high-haze ZnO pyramidal textures directly grown on a TCO substrate and the light-trapping effect in Cu2O solar cells. *J. Mater. Chem. C* **2014**, *2*, 2908−2917.
(15) Duan, X.; Zhang, X.; Zhang, Y. High Performance Organic-Nanostructured Silicon Hybrid Solar Cell with Modified Surface Structure. *Nanoscale Res. Lett.* **2018**, *13*, 283.
(16) Cheng, H.-M.; Chiu, W.-H.; Lee, C.-H.; Tsai, S.-Y.; Hsieh, W.-F. Formation of Branched ZnO Nanowires from Solvothermal Method and Dye-Sensitized Solar Cells Applications. *J. Phys. Chem. C* **2008**, *112*, 16359−16364.
(17) Liu, H.; Huang, Z.; Wei, S.; Zheng, L.; Xiao, L.; Gong, Q. Nano-structured electron transporting materials for perovskite solar cells. *Nanoscale* **2016**, *8*, 6209−6221.
(18) Peter Amalathas, A.; Alkaisi, M. M. Nanostructures for Light Trapping in Thin Film Solar Cells. *Micromachines* **2019**, *10*, 619.
(19) Zhou, L.; Xiang, H.-Y.; Zhu, Y.-F.; Ou, Q.-D.; Wang, Q.-K.; Du, J.; Hu, R.; Huang, X.-B.; Tang, J.-X. Multifunctional Silver Nanoparticle Interlayer-Modified ZnO as the Electron-Injection Layer for Efficient Inverted Organic Light-Emitting Diodes. *ACS Appl. Mater. Interfaces* **2019**, *11*, 9251−9258.
(20) Puyoo, E.; Rey, G.; Appert, E.; Consonni, V.; Bellet, D. Efficient Dye-Sensitized Solar Cells Made from ZnO Nanostructure Composites. *J. Phys. Chem. C* **2012**, *116*, 18117−18123.
(21) Consonni, V.; Briscoe, J.; Kärber, E.; Li, X.; Cossuet, T. ZnO nanowires for solar cells: a comprehensive review. *Nanotechnology* **2019**, *30*, 362001.
(22) Wibowo, A.; Marsudi, M. A.; Amal, M. I.; Ananda, M. B.; Stephanie, R.; Ardy, H.; Diguna, L. J. ZnO nanostructured materials for emerging solar cell applications. *RSC Adv.* **2020**, *10*, 42838−42859.
(23) Izaki, M.; Ohta, T.; Kondo, M.; Takahashi, T.; Mohamad, F. B.; Zamzuri, M.; Sasano, J.; Shinagawa, T.; Pauporté, T. Electrodeposited ZnO—Nanowire/Cu2O Photovoltaic Device with Highly Resistive ZnO Intermediate Layer. *ACS Appl. Mater. Interfaces* **2014**, *6*, 13461−13469.
(24) Liu, Y.; Gorla, C. R.; Liang, S.; Emanetoglu, N.; Lu, Y.; Shen, H.; Wraback, M. Ultraviolet detectors based on epitaxial ZnO films grown by MOCVD. *J. Electron. Mater.* **2000**, *29*, 69−74.
(25) Panth, M.; Cook, B.; Zhang, Y.; Ewing, D.; Tramble, A.; Wilson, A.; Wu, J. High-Performance Strain Sensors Based on Vertically Aligned Piezoelectric Zinc Oxide Nanowire Array/Graphene Nanohybrids. *ACS Appl. Nano Mater.* **2020**, *3*, 6711−6718.
(26) Zhou, C.; Ghods, A.; Yunghans, K.; Saravade, V.; Patel, P.; Jiang, X.; Kucukgok, B.; Lu, N.; Ferguson, I. ZnO for Solar Cell and Thermoelectric Applications. *SPIE* **2017**, *10105*, 225.
(27) Dahiya, A. S.; Sporea, R. A.; Poulin-Vittrant, G.; Alquier, D. Stability evaluation of ZnO nanosheet based source-gated transistors. *Sci. Rep.* **2019**, *9*, 2979.
(28) Hellstern, T. R.; Nielander, A. C.; Chakthranont, P.; King, L. A.; Willis, J. J.; Xu, S.; MacIsaac, C.; Hahn, C.; Bent, S. F.; Prinz, F. B.; Jaramillo, T. F. Nanostructuring Strategies To Increase the Photoelectrochemical Water Splitting Activity of Silicon Photocathodes. *ACS Appl. Nano Mater.* **2019**, *2*, 6−11.
(29) Mahala, C.; Sharma, M. D.; Basu, M. ZnO Nanosheets Decorated with Graphite-Like Carbon Nitride Quantum Dots as Photoanodes in Photoelectrochemical Water Splitting. *ACS Appl. Nano Mater.* **2020**, *3*, 1999−2007.
(30) Lecarme, L.; Consonni, V.; Lafolet, F.; Cossuet, T.; Mermoux, M.; Sauvage, F.; Nourdine, A.; Alloin, F.; Leprêtre, J.-C. ZnO Nanowires as a Promotor of High Photoinduced Efficiency and Voltage Gain for Cathode Battery Recharging. *ACS Appl. Energy Mater.* **2019**, *2*, 6254−6262.
(31) Vittal, R.; Ho, K.-C. Zinc oxide based dye-sensitized solar cells: A review. *Renewable Sustainable Energy Rev.* **2017**, *70*, 920−935.
(32) Özgür, Ü.; Alivov, Y. I.; Liu, C.; Teke, A.; Reshchikov, M. A.; Doğan, S.; Avrutin, V.; Cho, S.-J.; Morkoç, H. A comprehensive review of ZnO materials and devices. *J. Appl. Phys.* **2005**, *98*, 041301.
(33) Ellmer, K. Resistivity of polycrystalline zinc oxide films: current status and physical limit. *J. Phys. D: Appl. Phys.* **2001**, *34*, 3097−3108.
(34) Wang, Z. L. Piezoelectric Nanostructures: From Growth Phenomena to Electric Nanogenerators. *MRS Bull.* **2011**, *32*, 109−116.
(35) Liang, Z.; Gao, R.; Lan, J.-L.; Wiranwetchayan, O.; Zhang, Q.; Li, C.; Cao, G. Growth of vertically aligned ZnO nanowalls for inverted polymer solar cells. *Sol. Energy Mater. Sol. Cells* **2013**, *117*, 34−40.
(36) Xu, C.; Shin, P.; Cao, L.; Gao, D. Preferential Growth of Long ZnO Nanowire Array and Its Application in Dye-Sensitized Solar Cells. *J. Phys. Chem. C* **2010**, *114*, 125−129.
(37) Liu, L.; Hong, K.; Ge, X.; Liu, D.; Xu, M. Controllable and Rapid Synthesis of Long ZnO Nanowire Arrays for Dye-Sensitized Solar Cells. *J. Phys. Chem. C* **2014**, *118*, 15551−15555.
(38) Ameen, S.; Akhtar, M. S.; Song, M.; Shin, H. S. Vertically Aligned ZnO Nanorods on Hot Filament Chemical Vapor Deposition Grown Graphene Oxide Thin Film Substrate: Solar Energy Conversion. *ACS Appl. Mater. Interfaces* **2012**, *4*, 4405−4412.
(39) Woo Choi, H.; Lee, K.-S.; David Theodore, N.; Alford, T. L. Improved performance of ZnO nanostructured bulk heterojunction organic solar cells with nanowire-density modified by yttrium chloride introduction into solution. *Sol. Energy Mater. Sol. Cells* **2013**, *117*, 273−278.
(40) Chen, D.-W.; Wang, T.-C.; Liao, W.-P.; Wu, J.-J. Synergistic Effect of Dual Interfacial Modifications with Room-Temperature-Grown Epitaxial ZnO and Adsorbed Indoline Dye for ZnO Nanorod Array/P3HT Hybrid Solar Cell. *ACS Appl. Mater. Interfaces* **2013**, *5*, 8359−8365.
(41) Ji, G.; Zhao, W.; Wei, J.; Yan, L.; Han, Y.; Luo, Q.; Yang, S.; Hou, J.; Ma, C.-Q. 12.88% efficiency in doctor-blade coated organic solar cells through optimizing the surface morphology of a ZnO cathode buffer layer. *J. Mater. Chem. A* **2019**, *7*, 212−220.
(42) Parize, R.; Katerski, A.; Gromyko, I.; Rapenne, L.; Roussel, H.; Kärber, E.; Appert, E.; Krunks, M.; Consonni, V. ZnO/TiO2/Sb2S3 Core−Shell Nanowire Heterostructure for Extremely Thin Absorber Solar Cells. *J. Phys. Chem. C* **2017**, *121*, 9672−9680.
(43) Kösemen, A. Electrochemical growth of Y doped ZnO nanorods for use in inverted type organic solar cells as electron transport layer. *Mater. Res. Express* **2019**, *6*, 095024.
(44) Lee, Y. H.; Ha, M.; Song, I.; Lee, J. H.; Won, Y.; Lim, S.; Ko, H.; Oh, J. H. High-Performance Hybrid Photovoltaics with Efficient Interfacial Contacts between Vertically Aligned ZnO Nanowire Arrays and Organic Semiconductors. *ACS Omega* **2019**, *4*, 9996−10002.

https://doi.org/10.1021/acsomega.1c01654
ACS Omega 2021, 6, 32365−32378

(45) Portillo-Cortez, K.; Martínez, A.; Bizarro, M.; García-Sánchez, M. F.; Güell, F.; Dutt, A.; Santana, G. ZnO Nanowires/N719 Dye With Different Aspect Ratio as a Possible Photoelectrode for Dye-Sensitized Solar Cells. *Front. Chem.* **2021**, *8*, 604092.
(46) Zhang, Q.; Hou, S.; Li, C. Titanium Dioxide-Coated Zinc Oxide Nanorods as an Efficient Photoelectrode in Dye-Sensitized Solar Cells. *Nanomaterials* **2020**, *10*, 1598.
(47) Selim, M. S.; Elseman, A. M.; Hao, Z. ZnO Nanorods: An Advanced Cathode Buffer Layer for Inverted Perovskite Solar Cells. *ACS Appl. Energy Mater.* **2020**, *3*, 11781−11791.
(48) Qin, Y.; Chen, Y.; Cui, Y.; Zhang, S.; Yao, H.; Huang, J.; Li, W.; Zheng, Z.; Hou, J. Achieving 12.8% Efficiency by Simultaneously Improving Open-Circuit Voltage and Short-Circuit Current Density in Tandem Organic Solar Cells. *Adv. Mater.* **2017**, *29*, 1606340.
(49) Scharber, M. C.; Sariciftci, N. S. Efficiency of bulk-heterojunction organic solar cells. *Prog. Polym. Sci.* **2013**, *38*, 1929−1940.
(50) Mikhnenko, O. V.; Blom, P. W. M.; Nguyen, T.-Q. Exciton diffusion in organic semiconductors. *Energy Environ. Sci.* **2015**, *8*, 1867−1888.
(51) Bonasera, A.; Giuliano, G.; Arrabito, G.; Pignataro, B. Tackling Performance Challenges in Organic Photovoltaics: An Overview about Compatibilizers. *Molecules* **2020**, *25*, 2200.
(52) Xu, S.; Wang, Z. L. One-dimensional ZnO nanostructures: Solution growth and functional properties. *Nano Res.* **2011**, *4*, 1013−1098.
(53) Chevalier-César, C.; Capochichi-Gnambodoe, M.; Leprince-Wang, Y. Growth mechanism studies of ZnO nanowire arrays via hydrothermal method. *Appl. Phys. A: Mater. Sci. Process.* **2014**, *115*, 953−960.
(54) Greene, L. E.; Law, M.; Goldberger, J.; Kim, F.; Johnson, J. C.; Zhang, Y.; Saykally, R. J.; Yang, P. Low-Temperature Wafer-Scale Production of ZnO Nanowire Arrays. *Angew. Chem., Int. Ed.* **2003**, *42*, 3031−3034.
(55) Siva, V.; Park, K.; Kim, M. S.; Kim, Y. J.; Lee, G. J.; Kim, M. J.; Song, Y. M. Mapping the structural, electrical, and optical properties of hydrothermally grown phosphorus-doped ZnO nanorods for optoelectronic device applications. *Nanoscale Res. Lett.* **2019**, *14*, 110.
(56) Parize, R.; Garnier, J.; Chaix-Pluchery, O.; Verrier, C.; Appert, E.; Consonni, V. Effects of Hexamethylenetetramine on the Nucleation and Radial Growth of ZnO Nanowires by Chemical Bath Deposition. *J. Phys. Chem. C* **2016**, *120*, 5242−5250.
(57) Heo, S. N.; Ahmed, F.; Koo, B. H. Growth temperature dependent properties of ZnO nanorod arrays on glass substrate prepared by wet chemical method. *Ceram. Int.* **2014**, *40*, 5467−5471.
(58) Chevalier-César, C.; Capochichi-Gnambodoe, M.; Lin, F.; Yu, D.; Leprince-Wang, Y. Effect of growth time and annealing on the structural defect concentration of hydrothermally grown ZnO nanowires. *AIMS Mater. Sci.* **2016**, *3*, 562−572.
(59) Postels, B.; Wehmann, H.-H.; Bakin, A.; Kreye, M.; Fuhrmann, D.; Blaesing, J.; Hangleiter, A.; Krost, A.; Waag, A. Controlled low-temperature fabrication of ZnO nanopillars with a wet-chemical approach. *Nanotechnology* **2007**, *18*, 195602.
(60) Guillemin, S.; Consonni, V.; Appert, E.; Puyoo, E.; Rapenne, L.; Roussel, H. Critical Nucleation Effects on the Structural Relationship Between ZnO Seed Layer and Nanowires. *J. Phys. Chem. C* **2012**, *116*, 25106−25111.
(61) Vasireddi, R.; Javvaji, B.; Vardhan, H.; Mahapatra, D. R.; Hegde, G. M. Growth of zinc oxide nanorod structures: pressure controlled hydrothermal process and growth mechanism. *J. Mater. Sci.* **2017**, *52*, 2007−2020.
(62) Joo, J.; Chow, B. Y.; Prakash, M.; Boyden, E. S.; Jacobson, J. M. Face-selective electrostatic control of hydrothermal zinc oxide nanowire synthesis. *Nat. Mater.* **2011**, *10*, 596−601.
(63) Alshehri, N. A.; Lewis, A. R.; Pleydell-Pearce, C.; Maffeis, T. G. G. Investigation of the growth parameters of hydrothermal ZnO nanowires for scale up applications. *J. Saudi Chem. Soc.* **2018**, *22*, 538−545.
(64) Abdulrahman, A. F.; Ahmed, S. M.; Ahmed, N. M.; Almessiere, M. A. Enhancement of ZnO Nanorods Properties Using Modified Chemical Bath Deposition Method: Effect of Precursor Concentration. *Crystals* **2020**, *10*, 386.
(65) Boercker, J. E.; Schmidt, J. B.; Aydil, E. S. Transport Limited Growth of Zinc Oxide Nanowires. *Cryst. Growth Des.* **2009**, *9*, 2783−2789.
(66) Sakai, D.; Nagashima, K.; Yoshida, H.; Kanai, M.; He, Y.; Zhang, G.; Zhao, X.; Takahashi, T.; Yasui, T.; Hosomi, T.; Uchida, Y.; Takeda, S.; Baba, Y.; Yanagida, T. Substantial Narrowing on the Width of "Concentration Window" of Hydrothermal ZnO Nanowires via Ammonia Addition. *Sci. Rep.* **2019**, *9*, 14160.
(67) Coltrin, M. E.; Hsu, J. W. P.; Scrymgeour, D. A.; Creighton, J. R.; Simmons, N. C.; Matzke, C. M. Chemical kinetics and mass transport effects in solution-based selective-area growth of ZnO nanorods. *J. Cryst. Growth* **2008**, *310*, 584−593.
(68) Cheng, J. J.; Chuang, C.-H. M.; Hentz, O.; Rekemeyer, P. H.; Bawendi, M. G.; Gradečak, S. Dimension- and Surface-Tailored ZnO Nanowires Enhance Charge Collection in Quantum Dot Photovoltaic Devices. *ACS Appl. Energy Mater.* **2018**, *1*, 1815−1822.
(69) Ray, B.; Alam, M. A. Random vs regularized OPV: Limits of performance gain of organic bulk heterojunction solar cells by morphology engineering. *Sol. Energy Mater. Sol. Cells* **2012**, *99*, 204−212.
(70) Mukhopadhyay, S.; Narayan, K. S. Rationalization of donor-acceptor ratio in bulk heterojunction solar cells using lateral photocurrent studies. *Appl. Phys. Lett.* **2012**, *100*, 163302.
(71) Gaspar, H.; Figueira, F.; Pereira, L.; Mendes, A.; Viana, J.; Bernardo, G. Recent Developments in the Optimization of the Bulk Heterojunction Morphology of Polymer: Fullerene Solar Cells. *Materials* **2018**, *11*, 2560.
(72) Ma, W.; Tumbleston, J. R.; Ye, L.; Wang, C.; Hou, J.; Ade, H. Quantification of Nano- and Mesoscale Phase Separation and Relation to Donor and Acceptor Quantum Efficiency, Jsc, and FF in Polymer:Fullerene Solar Cells. *Adv. Mater.* **2014**, *26*, 4234−4241.
(73) Cao, W.; Xue, J. Recent progress in organic photovoltaics: device architecture and optical design. *Energy Environ. Sci.* **2014**, *7*, 2123−2144.
(74) Xiao, Z.; Sun, K.; Subbiah, J.; Qin, T.; Lu, S.; Purushothaman, B.; Jones, D. J.; Holmes, A. B.; Wong, W. W. H. Effect of molecular weight on the properties and organic solar cell device performance of a donor−acceptor conjugated polymer. *Polym. Chem.* **2015**, *6*, 2312−2318.
(75) Holmes, N. P.; Ulum, S.; Sista, P.; Burke, K. B.; Wilson, M. G.; Stefan, M. C.; Zhou, X.; Dastoor, P. C.; Belcher, W. J. The effect of polymer molecular weight on P3HT:PCBM nanoparticulate organic photovoltaic device performance. *Sol. Energy Mater. Sol. Cells* **2014**, *128*, 369−377.
(76) Gu, J.; Yuan, J.; Ma, W. Correlation between polymer molecular weight and optimal fullerene content in efficient polymer solar cells. *Org. Electron.* **2016**, *34*, 229−236.
(77) Kim, J.-H.; Gadisa, A.; Schaefer, C.; Yao, H.; Gautam, B. R.; Balar, N.; Ghasemi, M.; Constantinou, I.; So, F.; O'Connor, B. T.; Gundogdu, K.; Hou, J.; Ade, H. Strong polymer molecular weight-dependent material interactions: impact on the formation of the polymer/fullerene bulk heterojunction morphology. *J. Mater. Chem. A* **2017**, *5*, 13176−13188.
(78) McDowell, C.; Abdelsamie, M.; Toney, M. F.; Bazan, G. C. Solvent Additives: Key Morphology-Directing Agents for Solution-Processed Organic Solar Cells. *Adv. Mater.* **2018**, *30*, 1707114.
(79) Yan, Y.; Li, W.; Cai, F.; Cai, J.; Huang, Z.; Gurney, R. S.; Liu, D.; Lidzey, D. G.; Pearson, A. J.; Wang, T. Correlating Nanoscale Morphology with Device Performance in Conventional and Inverted PffBT4T-2OD:PC71BM Polymer Solar Cells. *ACS Appl. Energy Mater.* **2018**, *1*, 3505−3512.
(80) Ye, L.; Jing, Y.; Guo, X.; Sun, H.; Zhang, S.; Zhang, M.; Huo, L.; Hou, J. Remove the Residual Additives toward Enhanced Efficiency with Higher Reproducibility in Polymer Solar Cells. *J. Phys. Chem. C* **2013**, *117*, 14920−14928.

https://doi.org/10.1021/acsomega.1c01654
ACS Omega 2021, 6, 32365−32378

(81) Seo, M. H.; Kim, K. J.; Han, B. Y.; Anand, G. S.; Kim, S. H.; Lee, S. W.; Kang, S. W. Effect of Solvent Annealing for Efficient Polymer Solar Cells. *Adv. Mater. Res.* **2013**, *724*−*725*, 147−150.
(82) He, J.; Gao, P.; Liao, M.; Yang, X.; Ying, Z.; Zhou, S.; Ye, J.; Cui, Y. Realization of 13.6% Efficiency on 20 μm Thick Si/Organic Hybrid Heterojunction Solar Cells via Advanced Nanotexturing and Surface Recombination Suppression. *ACS Nano* **2015**, *9*, 6522−6531.
(83) Rahman, A.; Ashraf, A.; Xin, H.; Tong, X.; Sutter, P.; Eisaman, M. D.; Black, C. T. Sub-50-nm self-assembled nanotextures for enhanced broadband antireflection in silicon solar cells. *Nat. Commun.* **2015**, *6*, 5963.
(84) Garnett, E.; Yang, P. Light Trapping in Silicon Nanowire Solar Cells. *Nano Lett.* **2010**, *10*, 1082−1087.
(85) Alajlani, Y.; Placido, F.; Gibson, D.; Chu, H. O.; Song, S.; Porteous, L.; Moh, S. Nanostructured ZnO films prepared by hydrothermal chemical deposition and microwave-activated reactive sputtering. *Surf. Coat. Technol.* **2016**, *290*, 16−20.
(86) Erfan, M.; Gnambodoe-Capochichi, M.; Leprince-Wang, Y.; Marty, F.; Sabry, Y. M.; Bourouina, T. Nanowire Length, Density, and Crystalline Quality Retrieved from a Single Optical Spectrum. *Nano Lett.* **2019**, *19*, 2509−2515.
(87) Ho, P.-Y.; Thiyagu, S.; Kao, S.-H.; Kao, C.-Y.; Lin, C.-F. ZnO nanorod arrays for various low-bandgap polymers in inverted organic solar cells. *Nanoscale* **2014**, *6*, 466−471.
(88) Majidi, H.; Edley, M. E.; Spangler, L. C.; Baxter, J. B. Tailoring Absorber Thickness and the Absorber-Scaffold Interface in CdSe-Coated ZnO Nanowire Extremely Thin Absorber Solar Cells. *Electrochim. Acta* **2014**, *145*, 291−299.
(89) Ray, B.; Lundstrom, M. S.; Alam, M. A. Can morphology tailoring improve the open circuit voltage of organic solar cells? *Appl. Phys. Lett.* **2012**, *100*, 013307.
(90) Elumalai, N. K.; Uddin, A. Open circuit voltage of organic solar cells: an in-depth review. *Energy Environ. Sci.* **2016**, *9*, 391−410.
(91) Barshilia, H. C.; John, S.; Mahajan, V. Nanometric multi-scale rough, transparent and anti-reflective ZnO superhydrophobic coatings on high temperature solar absorber surfaces. *Sol. Energy Mater. Sol. Cells* **2012**, *107*, 219−224.

https://doi.org/10.1021/acsomega.1c01654
ACS Omega 2021, 6, 32365−32378